Greater committed warming after accounting for the pattern effect

Article *in* Nature Climate Change · February 2021

DOI: 10.1038/s41558-020-00955-x

4 authors, including:

Mark D. Zelinka
Lawrence Livermore National Laboratory
79 PUBLICATIONS **3,709** CITATIONS

SEE PROFILE

nature climate change

ARTICLES

https://doi.org/10.1038/s41558-020-00955-x

Greater committed warming after accounting for the pattern effect

Chen Zhou[1,2]✉, Mark D. Zelinka[3], Andrew E. Dessler[4] and Minghuai Wang[1,2]

Our planet's energy balance is sensitive to spatial inhomogeneities in sea surface temperature and sea ice changes, but this is typically ignored in climate projections. Here, we show the energy budget during recent decades can be closed by combining changes in effective radiative forcing, linear radiative damping and this pattern effect. The pattern effect is of comparable magnitude but opposite sign to Earth's net energy imbalance in the 2000s, indicating its importance when predicting the future climate on the basis of observations. After the pattern effect is accounted for, the best-estimate value of committed global warming at present-day forcing rises from 1.31 K (0.99–2.33 K, 5th–95th percentile) to over 2 K, and committed warming in 2100 with constant long-lived forcing increases from 1.32 K (0.94–2.03 K) to over 1.5 K, although the magnitude is sensitive to sea surface temperature dataset. Further constraints on the pattern effect are needed to reduce climate projection uncertainty.

The Earth's climate system gains energy by absorbing incoming solar radiation and loses energy by emitting thermal radiation back to the space. The absorbed solar radiation approximately equals the emitted thermal radiation at the top of atmosphere (TOA) when the Earth's climate system is in a quasi-equilibrium state. Since the Industrial Revolution, changes in greenhouse gases and aerosol concentration have perturbed the TOA radiative fluxes, resulting in a net energy flux into the climate system[1]. As the climate system warms in response to net positive radiative forcing, changes in surface temperature, air temperature, clouds, water vapour and surface albedo further modify the TOA energy fluxes, thereby radiatively damping the warming[2].

We can write the current energy imbalance as the sum of forcings and responses, that is

$$N = F + R_{\mathrm{fb}} \tag{1}$$

where F is the effective radiative forcing and R_{fb} is the offsetting change of TOA fluxes induced by warming of the climate system, including climate feedbacks. N is the net TOA energy imbalance. All anomalies are relative to the pre-industrial period.

Traditionally, the change of R_{fb} is calculated as the product of global mean surface temperature change and a climate feedback parameter λ. Using this approach, the IPCC AR5 (ref. [3]) described the Earth's energy budget with the following equation

$$N \approx F - \lambda \Delta T \tag{2}$$

where the effective climate feedback parameter λ, defined as the absolute value of total net feedback, is assumed to be a constant, and ΔT is change of global mean surface air temperature. However, it has been shown that λ is sensitive to the spatial pattern of sea surface temperature (SST) change[4–14], and the pattern of observed historical SST change has given rise to more negative cloud[5,8] and lapse rate feedbacks[10,15] than the SST change at $2\times CO_2$ equilibrium. Specifically, sea surface warming that is concentrated in warm regions of large-scale atmospheric ascent like the tropical western Pacific enhances Earth's albedo as well as its ability to radiate infrared energy to space. There is observational evidence for a pattern effect as well[10,16,17]. This means that the pattern effect must be considered in analyses of the Earth's energy imbalance.

We quantify the pattern effect as

$$P = R_{\mathrm{fb}} + \lambda_{\mathrm{lt}} \Delta T \tag{3}$$

where λ_{lt} is the climate feedback parameter under long-term, greenhouse gas-induced global warming and its value in climate models can be calculated from abrupt $4\times CO_2$ experiments[18] (Methods). The value of λ changes over time but the value of λ_{lt} is considered as a fixed value for the climate system. The values of R_{fb} can be calculated from Atmospheric Model Intercomparison Project (AMIP)-piForcing experiments, in which the model is forced by constant climate forcing and observed SST and sea ice[11] (Methods). The pattern effect is zero at equilibrium by this definition. A negative value of P indicates that the pattern effect cools Earth and vice versa.

Combining equations (1) and (3) gives us a modified energy balance equation

$$N = F - \lambda_{\mathrm{lt}} \Delta T + P \tag{4}$$

In this framework, the pattern effect P can be viewed as a pseudo-forcing composed of two parts[14]. One part is the unforced pattern effect induced by internal variability. Different patterns of warming over the historical period due to unforced variability lead to large differences between λ calculated over different decades. The other part is a forced pattern effect that causes λ over the historical period to be smaller than λ_{lt} due to differences between transient pattern of warming and the pattern of warming in response to $2\times CO_2$ (ref. [9]). When internal variability is taken into account, observed and simulated trends in SST patterns are consistent[19]. Note that the impact of internal variability on TOA fluxes affects both

[1]School of Atmospheric Sciences, Nanjing University, Nanjing, China. [2]Joint International Research Laboratory of Atmospheric and Earth System Sciences & Institute for Climate and Global Change Research, Nanjing University, Nanjing, China. [3]Cloud Processes Research and Modeling Group, Lawrence Livermore National Laboratory, Livermore, CA, USA. [4]Department of Atmospheric Sciences, Texas A&M University, College Station, TX, USA.
✉e-mail: czhou17@nju.edu.cn

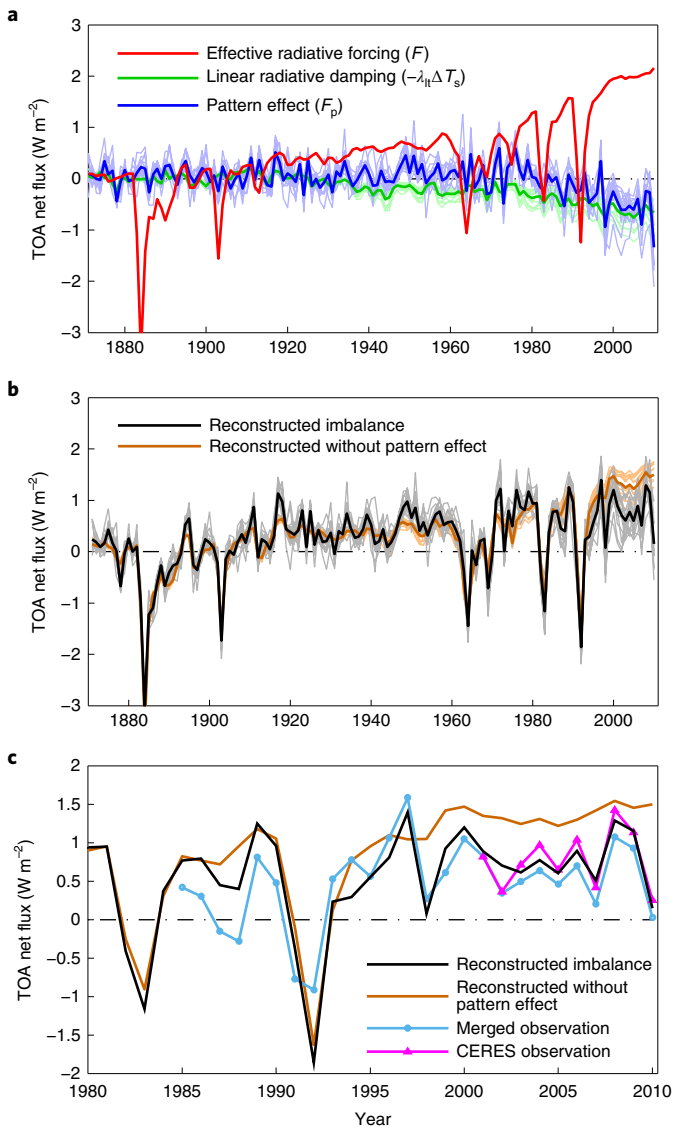

Fig. 1 | Attribution of the net TOA fluxes during 1871–2010. a, Time series of effective radiative forcing from IPCC AR5 (red), the linear radiative damping term ($-\lambda_{lt}\Delta T$, green) and the pattern effect term (blue). **b**, Time series of reconstructed TOA fluxes. The black line denotes the TOA fluxes reconstructed with equation (4) and the brown line denotes the TOA net flux estimated by ignoring the pattern effect ($F-\lambda_{lt}\Delta T$). **c**, Comparison of reconstructed TOA fluxes with observations. The magenta line denotes observed annual TOA net flux from CERES EBAF v.4.0 (ref. [21]) and the cyan line denotes net flux observations from merged radiation budget data v.3 (ref. [22]), which is calculated from CERES EBAF v.2.8 (ref. [42]) and ERBS wide field of view v.3 data[43]. Thin lines denote values calculated from individual models, while thick lines are model averages.

global mean temperature and the SST pattern, so the unforced component of the pattern effect accounts for only part of the internal variability-induced TOA radiative anomalies.

Our estimate of P comes from AMIP-piForcing simulations, so it is important to verify that the Earth's energy budget can be closed with the model-derived pattern effect. Figure 1 shows that the summation of climate forcings (F) from the IPCC AR5 (ref. [20]), linear radiative damping ($-\lambda_{lt}\Delta T$) and the pattern effect (P) from an ensemble of AMIP-piForcing simulations[11] closely matches the observed energy imbalance from the CERES EBAF observation dataset[21] and a merged CERES/ERBS radiation budget dataset that extends back to 1984[22].

The TOA imbalance calculated from equation (4) agrees with the observed energy imbalance, not only in the mean value during the 2000s but also in the interannual variations. Meanwhile, the TOA imbalance calculated assuming $P=0$ not only does not reproduce the correct magnitude but also does not reproduce year-to-year variations, indicating that the pattern effect is essential for accurately closing the Earth's energy budget. Our results are a complement to Andrews and Forster[23], who used the pattern effect to constrain F, yielding values consistent with the IPCC values we are using here.

We have also calculated the accumulated energy imbalance and the terms contributing to it, between 1961 and 2010. F is again from the IPCC AR5, and the pattern effect is calculated from individual AMIP-piForcing experiments (Methods). The observed changes in global heat content[24,25] are within the range of the accumulated energy influx for the whole period (Fig. 2). On the other hand, the cumulative energy influx calculated without the pattern effect is much larger than the observations. This further confirms that the pattern effect is crucial for closing the energy budget over the last several decades.

Estimates of committed warming with the pattern effect

The pattern effect is not only important for understanding the Earth's present energy budget but also for predicting future climate change. To illustrate the importance of the present-day SST pattern on future climate predictions, we now evaluate the impact of the pattern effect on estimates of committed warming under constant climate forcing scenarios[26].

We first consider a hypothetical future scenario, where climate forcing is held fixed as the present-day (2020) level until the climate system reaches equilibrium. The climate forcing in the hypothetical scenario relative to the pre-industrial period is

$$F = F_{ref} + \delta F \tag{5}$$

where F_{ref} is the effective total radiative forcing of the reference period (2005–2015) and $\delta F \approx 0.3$ W m^{-2} accounts for forcing by emissions from 2010 (the centre of the reference period) to 2020 to yield an up-to-date estimate of commitment[26]. At equilibrium, the Earth's energy imbalance N is zero and the pattern effect P is also zero as we define it, so equation (4) reduces to

$$0 = F - \lambda_{lt}\Delta T_a \tag{6}$$

where ΔT_a is the global mean surface temperature of the future scenario relative to pre-industrial. According to equations (5) and (6), the equilibrium committed warming with constant forcing F would therefore be

$$\Delta T_a = (F_{ref} + \delta F)/\lambda_{lt} \tag{7}$$

According to equation (4), the global mean surface temperature anomaly of the reference period (2005–2015) relative to pre-industrial period is

$$\Delta T_{ref} = (F_{ref} - N_{ref} + P_{ref})/\lambda_{lt} \tag{8}$$

where N_{ref} and P_{ref} are the TOA net flux and pattern effect during the reference period, respectively. Combining equations (7) and (8) we get

$$\Delta T_a = \Delta T_{ref} + (N_{ref} + \delta F)/\lambda_{lt} - P_{ref}/\lambda_{lt} \tag{9}$$

We refer to $-P_{ref}/\lambda_{lt}$ as the direct contribution of the pattern effect to equilibrium committed warming above today's temperature,

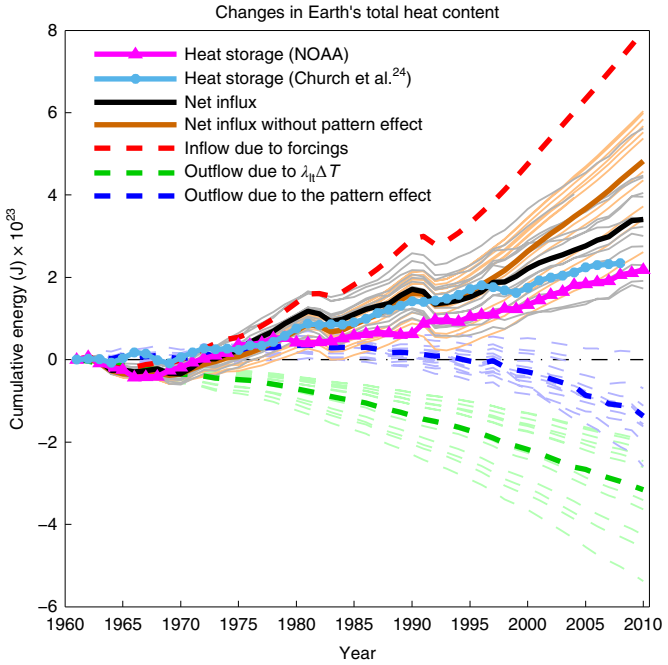

Fig. 2 | Cumulative energy flux into the Earth system during 1961–2010. The magenta and cyan lines are two estimates of the observed changes in the global heat content[24,25] (Methods), the black thick line is the net influx calculated from the reconstructed net energy imbalance of Fig. 1 and the brown thick line denotes net energy influx if the pattern effect is zero. The red, green and blue dashed lines denote individual contributors to the net energy influx. Thin lines denote values calculated from individual models, while thick lines are model averages.

which represents the contribution of the pattern effect when the committed warming is estimated from the reference period with given climate feedback parameter. Alternatively, one can also express the committed warming as

$$\Delta T_a = \frac{(F_{ref} + \delta F)}{(F_{ref} - N_{ref} + P_{ref})}\Delta T_{ref} \quad (10)$$

which highlights how the negative P_{ref} term enhances the equilibrium committed warming compared to $P_{ref}=0$.

Before the importance of the pattern effect on future climate predictions was recognized, many investigators solved for the climate feedback parameter λ_{lt} in equation (8) using historical observations with $P_{ref}=0$ (ref. [27]). We refer to such estimates as $\lambda_{lt,hist}$ and it was assumed that this was a good estimate of λ_{lt}. However, as we show below, ignoring the pattern effect yields an estimate of $\lambda_{lt,hist}$ that is larger (implying lower climate sensitivity) than λ_{lt} (ref. [11]). Using that $\lambda_{lt,hist}$ in equation (9) with $P_{ref}=0$ will then lead to a low-biased estimate of equilibrium committed warming.

We first estimate committed warming with forcing held fixed at present-day levels and no pattern effect. To do that, we calculate λ_{lt} from equation (8) with $P_{ref}=0$, basically equivalent to how $\lambda_{lt,hist}$ is normally calculated. Following ref. [26], we use $F_{ref}=2.16\pm0.59\,W\,m^{-2}$ ($1-\sigma$ uncertainty interval), $N_{ref}=0.71\pm0.06\,W\,m^{-2}$ and $\Delta T_{ref}=0.77\pm0.08\,K$ for 2005–2015. We find that $\lambda_{lt,hist}$ is 1.88 $W\,m^{-2}\,K^{-1}$ (0.66–3.27 $W\,m^{-2}\,K^{-1}$) with equation (8), which is similar to most previous traditional energy balance estimates[26,27]. Plugging that into equation (9) with $P_{ref}=0$ yields equilibrium committed warming ΔT_a of 1.31 K (0.99–2.33 K, 5th–95th percentile). This value is below the Paris Agreement's aspirational goal of 1.5 °C and is consistent with ref. [26].

Table 1 | AMIP-piForcing models used in this study

Model name	λ_{lt} ($W\,m^{-2}\,K^{-1}$)	ECS (K)	P ($W\,m^{-2}$)
CAM4	1.23	2.90	−0.77
CAM5.3	1.31	3.00	−0.59
CanESM5	0.65	5.64	−0.45
CESM2	0.63	5.15	−1.30
CNRM-CM6-1	0.74	4.90	−0.23
ECHAM6.3	1.36	3.01	−0.40
GFDL AM2.1	1.38	2.43	-
GFDL AM3	0.75	3.99	-
GFDL AM4	-	-	-
IPSL-CM6A-LR	0.75	4.56	−0.62
HadAM3	1.04	3.38	−0.56
HadGEM2	0.64	4.58	−0.60
HadGEM3-GC31-LL	0.63	5.55	−0.65
MRI-ESM2-0	1.10	3.13	−0.72
AMIP-piForcing ensemble	0.94	4.02	−0.63
CMIP5 models[40]	1.08	3.37	

CanESM5, CESM2, CNRM-CM6-1, HadGEM3-GC31-LL, MRI-ESM2-0 and IPSL-CM6A-LR are from CMIP6 (ref. [41]), and other models are from ref. [11]. The climate feedback parameter, ECS, and P during 2006–2010 are also listed in the table.

If we include a pattern effect of $P_{ref}=-0.63\pm0.27\,W\,m^{-2}$, which was inferred from the AMIP-piForcing experiments (Methods), the value of λ_{lt} estimated in equation (8) decreases to 1.06 $W\,m^{-2}\,K^{-1}$ (0.19–2.57 $W\,m^{-2}\,K^{-1}$), which is close to λ_{lt} estimates from climate models (Table 1) and the estimates of ref. [11]. It also falls near the middle of the range estimated from a meta-analysis of observational estimates of equilibrium climate sensitivity (ECS)[28], which suggests values of 0.79–1.61 $W\,m^{-2}\,K^{-1}$ for λ_{lt}. The value of ΔT_a estimated from equation (9) now rises to 2.31 K (1.26–10.3 K), which is substantially greater than the value estimated without the pattern effect. The best-estimate value is in excess of the 2 °C limit frequently viewed as the threshold for dangerous warming. More than half of this difference with the previous calculation is contributed by the direct effect $-P_{ref}/\lambda_{lt}$ (0.59 K when we set $\lambda_{lt}=1.06\,W\,m^{-2}\,K^{-1}$) in equation (9), and the rest (0.41 K) comes from the indirect effect of correcting the error in inferred $\lambda_{lt,hist}$ when the pattern effect is ignored (Fig. 3).

In addition to equilibrium committed warming with constant forcing, there are other definitions of committed warming[26,29]. Following ref. [26], we explore two other definitions. When the pattern effect is ignored, the equilibrium committed warming with constant long-lived forcing is estimated to be 1.59 K (0.91–4.45 K) and the committed warming with constant long-lived forcing by 2100 is 1.32 K (0.94–2.03 K), which is generally consistent with ref. [26]. After a pattern effect of $P_{ref}=-0.63\pm0.27\,W\,m^{-2}$ is fully accounted for, their values rise to 2.81 K (1.15–16.2 K) and 1.75 K (1.21–2.45 K), respectively (Methods).

Lewis and Mauritsen[30] suggested that the pattern effect is much weaker when the SST from HadISST[31] rather than AMIPII SST[32] are used in AMIP-piForcing runs. To examine the sensitivity to dataset used in the AMIP-piForcing runs, we carried out three experiments with CAM5.3 (ref. [33]) driven by HadISST SSTs and sea ice (CAM5.3 HadISST-piForcing experiments). The mean value of P between 2006 and 2010 is $-0.33\,W\,m^{-2}$ averaged across the three HadISST-piForcing experiments, which is weaker than the $-0.59\,W\,m^{-2}$ calculated from three CAM5.3 AMIP-piForcing experiments. If we set the pattern effect to be $P_{ref}=-0.33\,W\,m^{-2}$, the committed warming with present-day forcing is 1.69 K (1.18–4.50 K),

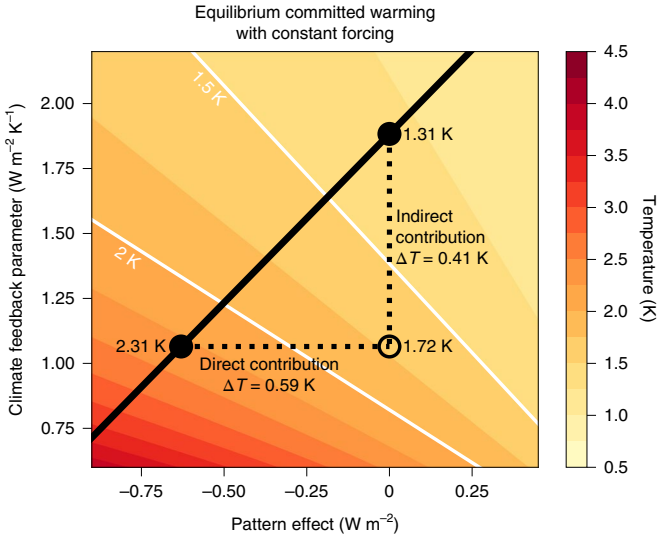

Fig. 3 | Impact of the pattern effect on equilibrium committed warming with constant forcing. Colours denote the committed warming for a range of P_{ref} and λ_{lt} values calculated with equation (9), and the two white contours represent the Paris Agreement thresholds. The black line denotes the relationship of P_{ref} and λ_{lt} constrained by equation (8). Values printed beside the two black markers denote the committed warming corresponding to $P_{ref}=0$ and $P_{ref}=-0.63$ W m^{-2}, respectively.

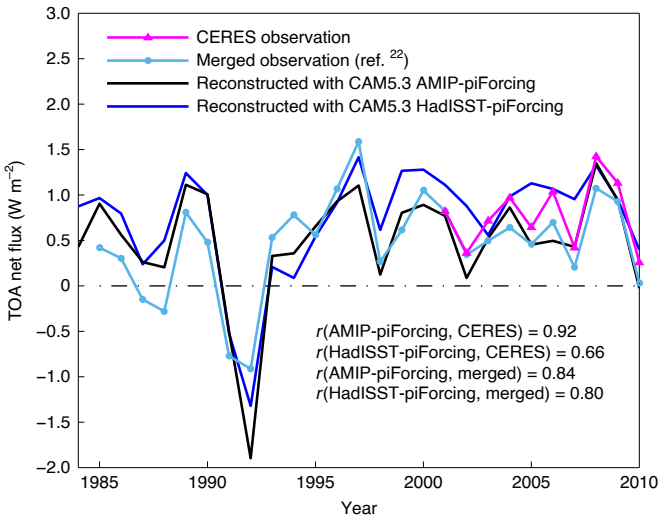

Fig. 4 | Comparison of TOA fluxes reconstructed with CAM5.3 experiments driven by different SST datasets. The TOA fluxes are reconstructed with equation (1), where the climate forcing is from IPCC AR5 and R_{fb} is from simulations. The black line is the ensemble mean value calculated from three CAM5.3 AMIP-piForcing experiments, which use prescribed AMIPII SST boundary conditions. The blue line is reconstructed with the ensemble mean value of three CAM5.3 HadISST-piForcing experiments, which use prescribed HadISST SST boundary conditions. The correlation coefficients between the time series of observations and reconstructed TOA fluxes, of which the corresponding P values are all below 0.05, are listed in the figure.

the equilibrium committed warming with constant long-lived forcing is 2.06 K (1.05–8.31 K), and the committed warming with constant long-lived forcing by 2100 is 1.62 K (1.13–2.24 K).

Therefore, we confirm that the committed warming estimated with zero pattern effect is substantially low biased compared to calculations that include the pattern effect. The magnitude of this bias depends on the SST dataset, with HadISST implying a smaller pattern effect and hence smaller committed warmings than the AMIPII dataset. However, we find that reconstructed TOA fluxes using CAM5.3 HadISST-piForcing experiments are less well correlated with observations than those in AMIP-piForcing experiments (Fig. 4), suggesting that committed warming estimates based on AMIP-piForcing experiments may be more reliable.

Implications and discussions

Properly accounting for the pattern effect has a major impact on the amount of carbon humans can emit before breaching any particular temperature threshold. Simple models frequently used to create the roadmap of decarbonization[34,35] typically do not include the pattern effect. It is expected that the pattern effect would be zero in the far future when the climate approaches equilibrium, so the transition from the current SST anomaly pattern to a more homogenous equilibrium pattern would result in an energy influx of ~0.63 ± 0.27 W m^{-2} in addition to forcing from additional greenhouse gases according to the AMIP-piForcing experiments. Considering that the effective radiative forcing of $2\times CO_2$ is 3.7 W m^{-2} (2.9–4.5 W m^{-2}) (ref. [36]), a reduction of ~47 ppm of CO_2 (14–86 ppm, the actual value might differ slightly because the forcing of CO_2 is nonlinear[37]) would be required to compensate for this pattern effect, which corresponds to ~100 petagrams of carbon (30–182 PgC). We are using a conversion factor of 2.12 PgC per ppm following ref. [38]. Therefore, consideration of the pattern effect would reduce the estimated remaining headroom to avoid exceeding target temperature thresholds[39] by about this much. Note that this value is ~53 PgC (43–67 PgC) if the pattern effect of −0.33 W m^{-2} derived from the CAM5.3 HadISST-piForcing experiment is used instead.

The pattern effect used in this study is derived from AMIP-piForcing experiments but its real-world strength could differ from that estimated in these idealized simulations. Uncertainty in the strength of the pattern effect substantially increases our uncertainty about future warming, and we hope our work motivates additional efforts to constrain it. As described here, this will have important consequences for understanding how much warming we are already committed to and how much of the carbon budget remains for us to have a reasonable chance to avoid the 1.5 °C and 2 °C climate thresholds set by the Paris Agreement.

Online content

Any methods, additional references, Nature Research reporting summaries, source data, extended data, supplementary information, acknowledgements, peer review information; details of author contributions and competing interests; and statements of data and code availability are available at https://doi.org/10.1038/s41558-020-00955-x.

Received: 15 April 2020; Accepted: 22 October 2020;
Published online: 04 January 2021

References

1. Trenberth, K. E., Fasullo, J. T., von Schuckmann, K. & Cheng, L. Insights into Earth's energy imbalance from multiple sources. *J. Clim.* **29**, 7495–7505 (2016).
2. Boucher, O. et al. in *Climate Change 2013: The Physical Science Basis* (eds Stocker, T. F. et al.) Ch. 7 (IPCC, Cambridge Univ. Press, 2013).
3. Stocker, T. F. et al. in *Climate Change 2013: The Physical Science Basis* (eds Stocker, T. F. et al.) 31–116 (IPCC, Cambridge Univ. Press, 2013).
4. Andrews, T., Gregory, J. M. & Webb, M. J. The dependence of radiative forcing and feedback on evolving patterns of surface temperature change in climate models. *J. Clim.* **28**, 1630–1648 (2015).
5. Zhou, C., Zelinka, M. D. & Klein, S. A. Impact of decadal cloud variations on the Earth's energy budget. *Nat. Geosci.* **9**, 871–874 (2016).

6. Gregory, J. M. & Andrews, T. Variation in climate sensitivity and feedback parameters during the historical period. *Geophys. Res. Lett.* **43**, 3911–3920 (2016).
7. Xie, S.-P., Kosaka, Y. & Okumura, Y. M. Distinct energy budgets for anthropogenic and natural changes during global warming hiatus. *Nat. Geosci.* **9**, 29–33 (2016).
8. Zhou, C., Zelinka, M. D. & Klein, S. A. Analyzing the dependence of global cloud feedback on the spatial pattern of sea surface temperature change with a Green's function approach. *J. Adv. Model. Earth Syst.* **9**, 2174–2189 (2017).
9. Armour, K. C. Energy budget constraints on climate sensitivity in light of inconstant climate feedbacks. *Nat. Clim. Change* **7**, 331–335 (2017).
10. Ceppi, P. & Gregory, J. M. Relationship of tropospheric stability to climate sensitivity and Earth's observed radiation budget. *Proc. Natl Acad. Sci. USA* **114**, 13126–13131 (2017).
11. Andrews, T. et al. Accounting for changing temperature patterns increases historical estimates of climate sensitivity. *Geophys. Res. Lett.* **45**, 8490–8499 (2018).
12. Silvers, L. G., Paynter, D. & Zhao, M. The diversity of cloud responses to twentieth century sea surface temperatures. *Geophys. Res. Lett.* **45**, 391–400 (2018).
13. Dessler, A. E., Mauritsen, T. & Stevens, B. The influence of internal variability on Earth's energy balance framework and implications for estimating climate sensitivity. *Atmos. Chem. Phys.* **18**, 5147–5155 (2018).
14. Dessler, A. E. Potential problems measuring climate sensitivity from the historical record. *J. Clim.* **33**, 2237–2248 (2019).
15. Dong, Y., Proistosescu, C., Armour, K. C. & Battisti, D. S. Attributing historical and future evolution of radiative feedbacks to regional warming patterns using a Green's function approach: the preeminence of the western Pacific. *J. Clim.* **32**, 5471–5491 (2019).
16. Fueglistaler, S. Observational evidence for two modes of coupling between sea surface temperatures, tropospheric temperature profile, and shortwave cloud radiative effect in the tropics. *Geophys. Res. Lett.* **46**, 9890–9898 (2019).
17. Leob, N. G. et al. New generation of climate models track recent unprecedented changes in earth's radiation budget observed by CERES. *Geophys. Res. Lett.* **47**, e2019GL086705 (2020).
18. Gregory, J. M. et al. A new method for diagnosing radiative forcing and climate sensitivity. *Geophys. Res. Lett.* **31**, L03205 (2004).
19. Olonscheck, D., Rugenstein, M. & Marotzke, J. Broad consistency between observed and simulated trends in sea surface temperature patterns. *Geophys. Res. Lett.* **47**, e2019GL086773 (2020).
20. Prather, M. G. et al. in *Climate Change 2013*: *The Physical Science Basis* (eds Stocker, T. F. et al.) 1395–1446 (IPCC, Cambridge Univ. Press, 2013).
21. Loeb, N. G. et al. Clouds and the Earth's radiant energy system (CERES) energy balanced and filled (EBAF) top-of-atmosphere (TOA) edition-4.0 data product. *J. Clim.* **31**, 895–918 (2018).
22. Allan, R. P. Decadal climate variability and the global energy balance. *Past Glob. Changes* **25**, 20–24 (2017).
23. Andrews, T. & Forster, P. M. Energy budget constraints on historical radiative forcing. *Nat. Clim. Change* **10**, 313–316 (2020).
24. Church, J. A. et al. Revisiting the Earth's sea-level and energy budgets from 1961 to 2008. *Geophys. Res. Lett.* **38**, L18601 (2011).
25. Levitus, S. et al. World ocean heat content and thermosteric sea level change (0–2000 m), 1955–2010. *Geophys. Res. Lett.* **39**, L10603 (2012).
26. Mauritsen, T. & Pincus, R. Committed warming inferred from observations. *Nat. Clim. Change* **7**, 652–655 (2017).
27. Forster, P. M. Inference of climate sensitivity from analysis of Earth's energy budget. *Annu. Rev. Earth Planet. Sci.* **44**, 85–106 (2016).
28. Sherwood, S. et al. An assessment of Earth's climate sensitivity using multiple lines of evidence. *Rev. Geophys.* **58**, e2019RG000678 (2020).
29. Smith, C. J. et al. Current fossil fuel infrastructure does not yet commit us to 1.5 °C warming. *Nat. Commun.* **10**, 101 (2019).
30. Lewis, N. & Mauritsen, T. Negligible unforced historical pattern effect on climate feedback strength found in HadISST-based AMIP simulations. *J. Clim.* https://doi.org/10.1175/JCLI-D-19-0941.1 (2020).
31. Rayner, N. A. et al. Global analyses of sea surface temperature, sea ice, and night marine air temperature since the late nineteenth century. *Geophys. Res.* **108**, 4407 (2003).
32. Hurrell, J. W., Hack, J. J., Shea, D., Caron, J. M. & Rosinski, J. A new sea surface temperature and sea ice boundary dataset for the Community Atmosphere Model. *J. Clim.* **21**, 5145–5153 (2008).
33. Neale, R. B. et al. *Description of the NCAR community atmosphere model (CAM 5.0) NCAR/TN-486+STR* (National Centre for Atmospheric Research, 2012).
34. Meinshausen, M., Raper, S. C. B. & Wigley, T. M. L. Emulating coupled atmosphere-ocean and carbon cycle models with a simpler model, MAGICC6 – Part 1: model description and calibration. *Atmos. Chem. Phys.* **11**, 1417–1456 (2011).
35. Rockström, J. et al. A roadmap for rapid decarbonization. *Science* **355**, 1269–1271 (2017).
36. Flato, G. et al. in *Climate Change 2013*: *The Physical Science Basis* (eds Stocker, T. F. et al.) Ch. 9 (IPCC, Cambridge Univ. Press, 2013).
37. Etminan, M., Myhre, G., Highwood, E. J. & Shine, K. P. Radiative forcing of carbon dioxide, methane, and nitrous oxide: a significant revision of the methane radiative forcing. *Geophys. Res. Lett.* **43**, 12614–12623 (2016).
38. Ciais, P. et al. in *Climate Change 2013*: *The Physical Science Basis* (eds Stocker, T. F. et al.) Ch. 6 (IPCC, Cambridge Univ. Press, 2013).
39. Zhou, T. & Chen, X. Uncertainty in the 2°C warming threshold related to climate sensitivity and climate feedback. *J. Meteorol. Res.* **29**, 884–895 (2015).
40. Andrews, T., Gregory, J. M., Webb, M. J. & Taylor, K. E. Forcing, feedbacks and climate sensitivity in CMIP5 coupled atmosphere–ocean climate models. *Geophys. Res. Lett.* **39**, L09712 (2012).
41. Eyring, V. et al. Overview of the coupled model intercomparison project phase 6 (CMIP6) experimental design and organization. *Geosci. Model Dev.* **9**, 1937–1958 (2016).
42. Loeb, N. G. et al. Observed changes in top-of-the-atmosphere radiation and upper-ocean heating consistent within uncertainty. *Nat. Geosci.* **5**, 110–113 (2012).
43. Wielicki, B. A. et al. Evidence for large decadal variability in the tropical mean radiative energy budget. *Science* **295**, 841–844 (2002).

Methods

Calculation of pattern effect. The change of TOA fluxes in response to observed SST and sea ice changes, ΔR_{fb}, is calculated as the change of TOA fluxes relative to the base period (1871–1880) in the AMIP-piForcing experiments, where the sea ice and SST are specified from observations and climate forcings are fixed at pre-industrial level. The AMIP-piForcing ensemble consists of 14 models, of which eight are from ref. [11] and six are from the Coupled Model Intercomparison Project Phase 6 (CMIP6) archive. Considering that the value of effective forcing during the base period is 0.04 W m^{-2} and the net energy imbalance is set to be 0.08 W m^{-2} during 1860–1879 in ref. [44], we set the value of R_{fb} during the base period to be $R_{fb,baseperiod} = 0.04$ W m^{-2}. The value of R_{fb} at each year is calculated as the summation of ΔR_{fb} and $R_{fb,baseperiod}$. (Note that if we set $R_{fb,baseperiod} = 0$, R_{fb} at each year would be more negative than values reported in the paper.) The value of λ_{lt} of each model is calculated from abrupt $4\times CO_2$ experiments as the regression slope of TOA net flux against global mean surface temperature during years 1–150, following ref. [18]. From this information, the values of P can be calculated with equation (3), where ΔT is calculated as the change of global mean surface air temperature relative to the base period. It is worth noting that the climate feedback parameter is smaller (less negative net feedback) during years 21–150 than that during years 1–20 (ref. [4]), so calculating λ_{lt} from years 21–150 instead of years 1–150 results in a larger, more negative pattern effect.

The λ_{lt} parameter of GFDL AM4 is unavailable and the GFDL AM2.1 and AM3 AMIP runs end in 2005, so some values are missing in Table 1.

Pattern effect after 2011. The AMIP-piForcing experiments of ref. [11] end in 2010 and it is important to know whether the pattern effect has changed significantly after 2011. We run three additional AMIP-piForcing experiments with CAM5.3 (ref. [33]) over the period 1871–2017. The average value of P in these runs is −0.59 W m^{-2} during 2006–2010, −0.64 W m^{-2} during 2006–2015 (reference period for committed warming calculations) and −0.56 W m^{-2} during 2011–2017 in these additional CAM5.3 AMIP-piForcing experiments. This shows that P estimated using runs ending in 2010 are similar to those ending in 2015, so the value of P during 2006–2010 in AMIP-piForcing experiments is used as P_{ref} when we evaluate the impact of pattern effect on committed warming.

Global heat content data. The dataset from ref. [24] contains global heat content changes in ocean, ice, atmosphere and land, while the heat content of NOAA[25] contains ocean heat content only. The total heat content of ref. [24] is used in Fig. 2. Considering that uncertainties of global heat content changes are dominated by the ocean, we calculated another total heat content time series by adding up the ocean heat content change from NOAA with ice, atmosphere and land heat content from ref. [24] and noted it as 'NOAA' in Fig. 2. The data of ref. [24] ends in 2008, so we extended the air, land and ice heat content to 2010 using linear extrapolation. The extrapolation error of air, land and ice heat content is expected to have little impact on the total heat content because changes in ocean heat content are much larger than those of the air, land and ice.

Uncertainty intervals. The uncertainty intervals in this paper are calculated with bootstrapping. Variables with negligible skewness were sampled with normal distribution and variables with strong skewness were transformed to an alternative variable with weak skewness before sampling. Considering that the value of λ_{lt} should be positive, random samples leading to negative λ_{lt} are excluded when we estimate the uncertainty intervals. The values reported before the uncertainty intervals are best-estimate values and they are not affected by this truncation.

Committed warming with constant long-lived forcing. In the absence of fossil fuel emissions, aerosols and short-lived climate forcings would rapidly decrease, so we also consider a future scenario where the concentration of long-lived forcers (well-mixed greenhouse gases excluding fossil fuel-induced methane) remain fixed at present-day level, while the concentration of aerosols and short-lived greenhouse gases is at the pre-industrial level[26]. The climate forcing in this future scenario relative to the pre-industrial period is

$$F_{LLCF} = F_{ref} + \delta F - F_{aero} - F_{SLCF} \quad (11)$$

where F_{aero} and F_{SLCF} are the effective aerosol radiative forcing and short-lived climate forcing at the reference period (2005–2015), respectively. According to ref. [26], $F_{SLCF} = 0.36$ W m^{-2} (0.17–0.56 W m^{-2}) and $F_{aero} = -0.9$ W m^{-2} (−1.9 to −0.1 W m^{-2}) during the reference period, then the best-estimate value of F_{LLCF} can be calculated from equation (11) (3.0 W m^{-2}) but its uncertainty interval is difficult to estimate from equation (11) with bootstrapping because the correlation between the uncertainties of F_{aero} and F_{ref} is unknown. Alternatively, we added the forcing from well-mixed greenhouse gases (excluding fossil fuel-induced methane, which accounts for 29% of total methane according to ref. [26]) in IPCC AR5 (ref. [3]) with δF, and estimate that the value of F_{LLCF} is 3.0 W m^{-2} (2.7–3.3 W m^{-2}). Following equation (7), the equilibrium committed warming with this level of forcing is

$$\Delta T_c = F_{LLCF}/\lambda_{lt} = (F_{ref} + \delta F - F_{aero} - F_{SLCF})/\lambda_{lt} \quad (12)$$

Combining equations (8) and (12) we have

$$\Delta T_c = \Delta T_{ref} + (N_{ref} + \delta F - P_{ref} - F_{aero} - F_{SLCF})/\lambda_{lt} \quad (13)$$

If we set $P_{ref} = 0$, the value of ΔT_c is 1.59 K (0.91–4.45 K). If we set $P_{ref} = -0.33$ W m^{-2} (derived from CAM5.3 HadISST-piForcing), the value of ΔT_c increases to 2.06 K (1.05–8.31 K). When the pattern effect derived from AMIP-piForcing experiments $P_{ref} = -0.63 \pm 0.27$ W m^{-2} is accounted for, the value of ΔT_c increases to 2.81 K (1.15–16.2 K).

The pattern effect is also important in estimating the committed warming at the end of the twenty-first century. We assume that the average value of pattern effect is zero during the projected period. Following ref. [26], we assume that the centennial response to present-day forcing is consistent with the response to historical forcing, and the centennial commitment warming with constant long-lived forcing can be approximated using transient climate response (TCR)

$$\Delta T_d = \Delta T_{ref} + (N_{ref} + \delta F - P_{ref} - F_{aero} - F_{SLCF})\frac{TCR}{F_{2\times}} \quad (14)$$

$F_{2\times}$ is the effective forcing from a doubling of CO_2 concentration and is estimated to be 3.7 W m^{-2} (2.9–4.5 W m^{-2}) according to ref. [36]. If the pattern effect is completely ignored, the value of TCR is estimated to be 1.32 K (0.88–2.36 K), so the value of ΔT_d is estimated to be 1.32 K (0.94–2.03 K). If the pattern effect is considered, the estimated TCR increases to 1.67 K (1.17–2.16 K) according to ref. [45] and the estimated ΔT_d from equation (14) increases to 1.62 K (1.13–2.24 K) when the pattern effect derived from CAM5.3 HadISST-piForcing experiments is used and increases to 1.75 K (1.21–2.45 K) when the pattern effect derived from AMIP-piForcing experiments is used.

Data availability

All observational data and AMIP-piForcing experiment data in Table 1 are publicly available online, as described in Methods. In addition, results of the idealized experiments carried out in this study are available from the corresponding author upon request.

Code availability

The code of CESM1.2-CAM5.3 model used in this paper can be downloaded from http://www.cesm.ucar.edu/models/cesm1.2/. Codes for plotting figures are available from the corresponding author upon request.

References

44. Otto, A. et al. Energy budget constraints on climate response. *Nat. Geosci.* **6**, 415–416 (2013).
45. Jiménez-de-la-Cuesta, D. & Mauritsen, T. Emergent constraints on Earth's transient and equilibrium response to doubled CO_2 from post-1970s global warming. *Nat. Geosci.* **12**, 902–905 (2019).

Acknowledgements

C.Z. was supported by NSFC grant no. 41875095. A.E.D. was supported by NSF grant nos. AGS-1661861 and AGS-1841308, both to Texas A&M University. M.D.Z. worked under the auspices of the US Department of Energy (DOE), Lawrence Livermore National Laboratory under contract no. DE-AC52-07NA27344 and was supported by the Regional and Global Model Analysis Program of the Office of Science at the DOE. M.W. was supported by Minister of Science and Technology of China grant nos. 2017YFA0604002 and 2016YFC0200503, and NSFC grant nos. 91744208, 41575073 and 41621005. This research is also supported by the Collaborative Innovation Center of Climate Change, Jiangsu Province. The numerical simulations in this paper were done on the computing facilities in the High Performance Computing Center of Nanjing University. Correspondence and requests for materials should be addressed to C.Z.

Author contributions

C.Z. performed the analysis. The paper was discussed and written by all authors.

Competing interests

The authors declare no competing interests.

Additional information

Correspondence and requests for materials should be addressed to C.Z.

Peer review information *Nature Climate Change* thanks Jonah Bloch-Johnson, Diego Jiménez-de-la-Cuesta and the other, anonymous, reviewer(s) for their contribution to the peer review of this work.

Reprints and permissions information is available at www.nature.com/reprints.